New insights into the earliest phases of low-mass star formation with the Herschel Space Observatory

J. Di Francesco[*]
National Research Council of Canada, Victoria, BC, Canada

Abstract. The *Herschel Space Observatory* has been revolutionizing our understanding of the the earliest phases of star formation. In this contribution, we describe early results from the Gould Belt Survey, a *Herschel* Key Project to map 15 nearby molecular clouds in continuum emission from 70 μm to 500 μm. In particular, I describe how the sensitive and wide maps of the Aquila Rift have strongly confirmed the similarity between the shapes of the stellar Initial Mass Function and the prestellar core mass function (CMF). Also, the *Herschel* map sensitivity to larger scale emission has revealed that prestellar cores form almost exclusively within dense filaments that exceed a critical mass per unit length defined by temperature (and gravity). Finally, filaments in three clouds, IC 5146, Polaris and Aquila, are found to have similar widths of ~0.1 pc, approximately the scale where the turbulent velocity equals the sound speed of 10 K gas. This common width suggests filaments themselves are formed through collisional shocks of turbulent flows and evolve in quasi-virial balance through mass accretion.

Keywords : far-infrared/submillimetre – prestellar cores – *Herschel Space Observatory*

1.   Introduction

The transition between diffuse molecular clouds and protostars are the "starless cores," dense gas pockets of size ~0.1 pc and mean density ~10^4 cm^{-3} that are built up within these larger clouds (for recent reviews see Di Francesco et al. 2007; Ward-Thompson et al. 2007; Bergin & Tafalla 2007). Low-mass stars (i.e., those with M < 8 M$_\odot$)

[*]email: james.difrancesco@nrc-cnrc.gc.ca

form out of such cores when they become unable to resist their own gravity and collapse. Hence, starless cores represent the earliest phase of low-mass star formation, and studying them reveals the initial conditions of low-mass stellar evolution. The subset of starless cores that are most likely to form stars are those that are gravitationally bound, and these have been termed "prestellar cores" (see Di Francesco et al.)

With high column densities (i.e., $A_V > 10$) and no internal heating sources, prestellar cores can be among the coldest objects in the universe. For example, they have surface temperatures of 10-20 K but can have central temperatures of only ~5-6 K (Evans et al. 2001; Crapsi et al. 2007). Accordingly, the peak of thermal emission from dust particles within cores lies at far-infrared and submillimetre wavelengths, i.e., $\lambda = 100$-$500\ \mu$m. Over the last 15 years, wide-field bolometric arrays like SCUBA on the James Clerk Maxwell Telescope or Bolocam on the Caltech Submillimeter Observatory enabled the first limited censuses of starless cores by detecting their continuum emission from dust within nearby molecular clouds (e.g., Motte, André & Neri 1998; Johnstone et al. 2000, 2004; Kirk et al. 2006; Enoch et al. 2008), typically at angular resolutions of 10-40″ or < 0.1 pc at the distance of Orion.

Given high atmospheric opacities over the range of wavelengths where cores are brightest, ground-based core surveys sampled thermal emission between 850 μm and 1300 μm, i.e., at wavelengths far down the Rayleigh-Jeans tails of the core spectral energy distributions (SEDs) but still accessible from dry locations. These surveys also had to contend with bright emission from the atmosphere itself. Such emission could be removed effectively by "chopping," i.e., rapidly oscillating a nutating secondary mirror and subtracting off-target data from on-target data. Chopping spatially filters the final maps, however, removing emission on scales larger than the "chop throw," i.e., the angular separation of on- and off-source positions that was on the order of ~1′. Combined, these realities limited the sensitivity of these investigations, especially on large scales within these clouds, but the brightest and most compact cores were well sampled.

An imporant result from submillimetre/millimetre ground-based surveys of nearby clouds was the similarity of the core mass functions (CMFs) of their respective populations to the Initial Mass Function (IMF) of stars, especially at their respective high mass ends. For example, the high-mass slopes of CMFs were typically within errors of that of the IMF at higher masses, i.e., $\alpha \approx 1.35$ (Salpeter 1955). This similarity suggests that stars obtain their respective masses from physical processes within molecular clouds that organize material first into star-forming units, i.e., cores. Due to low sample sizes (e.g., <100 cores), however, this similarity was not very robust (see Sadavoy et al. 2010). Nevertheless, the implications of the similarities between the CMF and IMF have been a matter of wide discussion within the star-formation community, see, e.g., Alves et al. (2007), Swift & Williams (2008), Reid et al. (2010), Ananthpindika (2011), among others over the last decade.

2.   Herschel and the Gould Belt Survey

On 14 May 2009, the European Space Agency (ESA) launched the 3.5-m diameter *Herschel Space Observatory*, the world's widest space telescope to date (see Pilbratt et al. 2010). *Herschel* was designed to ameliorate the difficulties of observing cold objects described above by being able to probe without spatial filtering far-infrared/submillimetre wavelengths unobservable from the ground. *Herschel* can obtain such data using two camera-like instruments, the Photodetector Array Camera and Spectrometer (PACS; Poglitsch et al. 2010) and the Spectral and Photometric Imaging REceiver (SPIRE; Griffin et al. 2010). PACS can detect simultaneously 70 μm or 100 μm and 160 μm emission and SPIRE can detect simultaneously 250 μm, 350 μm, and 500 μm emission. Both instruments can be operated in parallel to map simultaneously large regions of the sky at five wavelengths that bracket the SED peaks of cold objects like starless cores. For high sensitivity, PACS and SPIRE must be cryogenically cooled and *Herschel*'s cryogens are expected to last 3.5 years in total, i.e., until the end of 2012.

One-third of *Herschel*'s available observing time was offered to the teams who built its instrument suite. (The remaining two-thirds has been offered to the global community through peer-reviewed proposal calls.) These teams were encouraged to devise Key Projects, where >100 hours could be devoted to address significant problems in astrophysics. Specifically, members of the SPIRE and PACS teams devoted 492 hours to an extensive survey to map the full extents of 15 nearby molecular clouds within 500 pc of the Sun with both instruments, i.e., typically where $A_V > 1$-3 with SPIRE and PACS in parallel and $A_V > 6$ with PACS alone. Since most of these sampled clouds (including Orion, Perseus, Taurus and Ophiuchus) occupy a narrow locus across the sky now called the Gould Belt (cf. Gould 1879), this survey has been dubbed the *Herschel* Gould Belt Survey (GBS). The co-PIs of the GBS are Ph. André (CEA-Saclay) and P. Saraceno (IFSI-Rome), and GBS members are based in France, Italy, the UK, Canada, Germany, Spain, Belgium, Sweden, and China. This paper will discuss the first results from the GBS and the profound implications they have already revealed about low-mass star formation.

3.   Cores and filaments in the Aquila Rift

Fig. 1 (left) shows a 10 deg^2 image of the Aquila Rift cloud at 230 pc obtained by the GBS at 70 μm (blue), 160 μm (green), and 500 μm (red), as described by André et al. (2010), Könyves et al. (2010) and Bontemps et al. (2010). The image reveals the wealth of structure typically seen in nearby clouds by *Herschel* with PACS and SPIRE in parallel. The compact blue features indicate warmer dust associated with the young clusters W40 (north) and MWC 297 (south) but the image is dominated by red features indicating cold dust, many of which are compact. A preliminary extraction of sources using a new multi-wavelength/multi-scale structure identification algorithm called *getsources* (Men'shchikov et al. 2010) found 541 cores that could
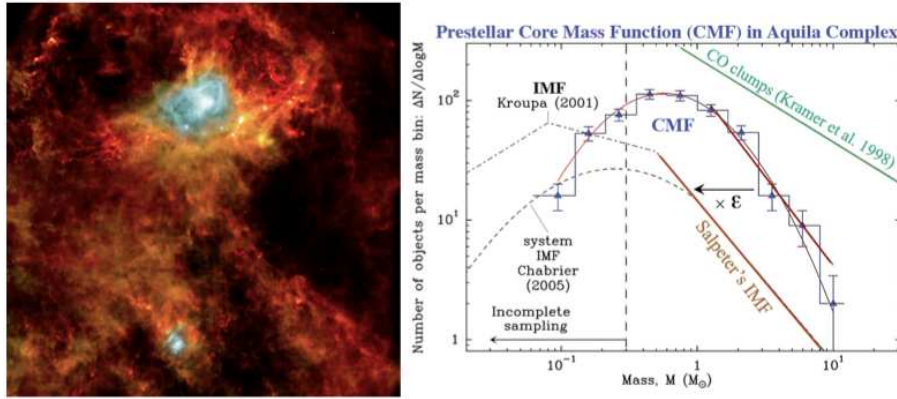
Figure 1. (*left*) A 10 deg^2 image of the Aquila Rift imaged at 70 μm (blue), 160 μm (green), and 500 μm (red) with the PACS and SPIRE instruments of *Herschel*. (*right*) A histogram showing the prestellar core mass function derived from 541 objects identified the *Herschel* data (blue) overlaid with a lognormal fit (thin red) and a linear slope at high masses (thick red). For comparison, the stellar (Salpeter 1955) and CO clump mass function (Kramer et al. 1998) slopes are shown (orange and green respectively). The IMFs determined by Kroupa (2001) and Chabrier (2005) are also shown (dash-dotted and dotted lines respectively). (Panels from André et al. 2010.)

be considered "prestellar" in nature. Though no line widths have been observed towards these objects (yet), they appear gravitationally bound; they have high degrees of central concentration (i.e., $N_{H_2}/ < N_{H_2} > \sim 4$ on average) and have masses and sizes similar to those of Bonnor-Ebert spheroids.

Fig.1 (right) shows the CMF constructed with the 541 prestellar cores in Aquila. The sample used for this CMF is a factor of 5-6 larger than that used in previous CMF analyses. Immediately, the Aquila data confirm strongly the similarity between the CMF and IMF. The CMF has a lognormal shape similar to those of the IMFs found by Kroupa (2001) and Chabrier (2005). Moreover, the slope of the Aquila CMF is $\sim 1.5 \pm 0.2$, consistent with the Salpeter slope of 1.35 but with smaller errors than found previously. So similar are the IMF and CMF in shape, it is tempting to imagine an efficiency factor, $\epsilon = 0.2\text{-}0.4$, directly relates the two distributions. Further work, however, is required to substantiate this connection, e.g., by pushing the completeness level to lower masses and assessing whether or not the CMF truly peaks at 0.3-0.5 M$_\odot$).

The wealth of the Herschel data goes beyond the identification of CMFs in nearby clouds, and provides for the first time a glimpse into the necessary requirements for core formation itself. Fig.2 (left) shows a map of the column densities in Aquila, determined using the Herschel data themselves by fitting SEDs for temperatures and converting intensities on a pixel-by-pixel basis. (A dust opacity power-law with exponent $\beta = 2$ (Hildebrand 1983) was assumed.) The panel also shows the locations of
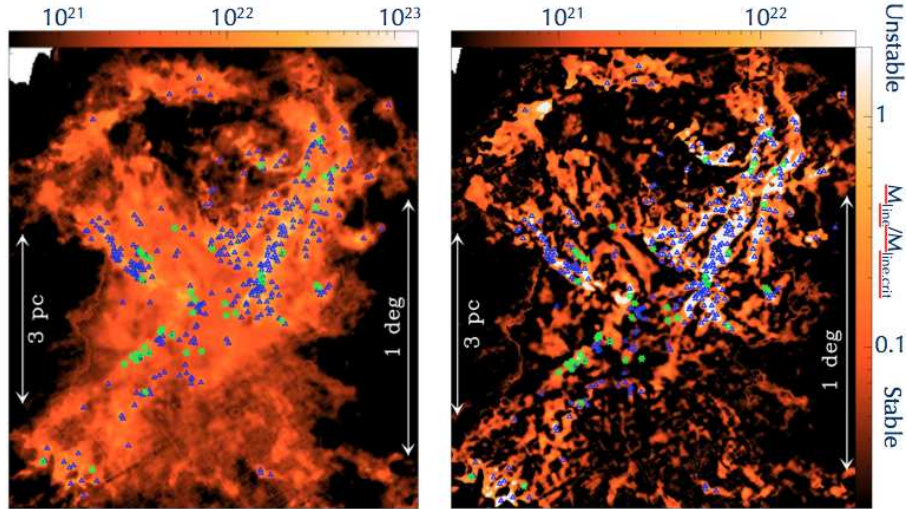
Figure 2. (*left*) Column density map of the Aquila Rift obtained using *Herschel* data to fit temperatures on a pixel-by-pixel bases while assuming a dust opacity power-law exponent of β = 2. The colour scale ranges from $\sim 2 \times 10^{20}$ cm^{-2} to $\sim 1.5 \times 10^{23}$ cm^{-2}. The blue triangles and green stars represent the respective positions of prestellar cores and Class 0 objects identified in the field, again through *Herschel* data. (*right*) Curvelet component map of the column densities across Aquila, with colour scale defined so that white areas represent locations where the mass per unit length exceeds the critical value of ~ 15 M$_\odot$ pc^{-1} for T = 10 K predicted by Inutsuka & Miyama (1997). (Panels are from André et al. 2010.)

prestellar cores and protostars in Aquila overlaid on the column densities, and one can see immediately that these lie in linear arrangements. Fig.2 (right) shows the same objects overlaid on a column density map of Aquila where only intermediate spatial scales have been retained after a curvelet/wavelet spatial decomposition. (Ambient emission from the cloud on large scales and compact emission from cores on small scales have been removed.) This decomposition reveals that Aquila is permeated by long filamentary structures. Moreover, the panel reveals that the Class 0 objects and prestellar cores individually lie on top of such structures, and also they collectively are associated with some of these. Together, these associations suggest a strong connection between core formation and filamentary structures.

Why do cores form in some filaments but not others? Fig.2 (right) has had its column densities converted to a mass per unit length scale using the width of the associated filament as a proxy for the depth. Moreover, these quantities have been normalized to a critical mass per unit length suggested for non-magnetized filaments by Inutsuka & Miyama (1997; cf. Ostriker 1964) equal to $2c_s^2/G = 15$ M$_\odot$ pc^{-1} at 10 K. As can be seen, prestellar cores and Class 0 objects are located predominantly towards filaments whose masses per unit length exceed this critical value. From this, we conclude the self-gravitating prestellar cores (and protostars) can only form within
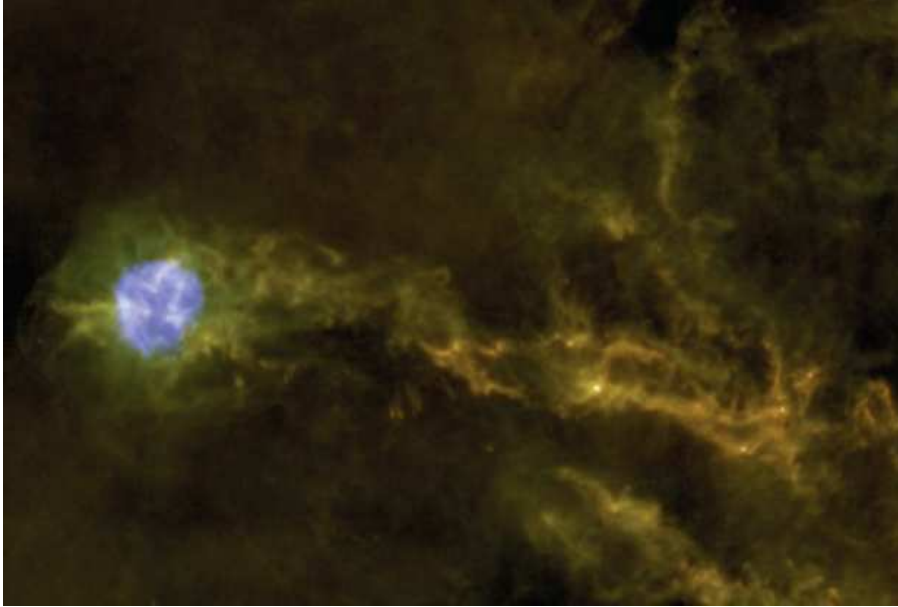
Figure 3. Three colour image of IC 5146 in 70 μm (blue), 160 μm (green), and 500 μm (red). The blue feature to the left is the Coocon Nebula. (Panel from Arzoumanian et al. 2011.)

filaments that exceed this critical value; conversely, any density enhancements in filaments of lower mass per unit length are unable to persist or grow into cores. The simplicity of the critical threshold is striking, as it only depends on the local temperature (and gravity). In total, the picture emerging from Aquila is one where turbulence appears to form complex networks of filaments within clouds, and only a subset of these form cores (and stars) once gravity becomes dominant. (Indeed, this picture also explains *Herschel* GBS observations of the Polaris Flare cloud where filaments but no prestellar cores or YSOs are found; these data are not shown but see Ward-Thompson et al. 2010, Miville-Deschênes et al. 2010 for details. For low-extinction Polaris, the masses per unit length do not approach the critical mass per unit length value at any location, easily explaining its lack of prestellar cores or protostars.)

4. Constant filament width in IC 5146, Aquila and Polaris

Fig. 3 shows the 1.6 deg^2 *Herschel* image of the molecular cloud IC 5146, located at 460 pc (Arzoumanian et al. 2011), obtained at 70 μm (blue), 250 μm (green), and 500 μm (red). In this field, the blue region at left indicates warm dust illuminated by the Cocoon Nebula, an HII region illuminated by the B0 V star BD+46°3474. As seen for Aquila, the region of warm dust is highly localized, and emission from the cloud is dominated by cold filamentary structure.
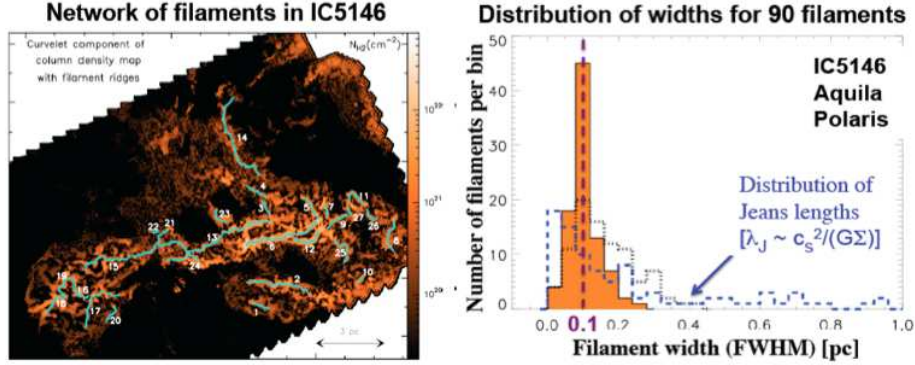
Network of filaments in IC5146

Distribution of widths for 90 filaments

Figure 4. (*left*) Curvelet component of the column densities across the IC 5146 molecular cloud, overlaid by linear features indicating the positional loci of maximum column density associated with the filament identified using DisPerSe. The colour scale ranges from $\sim 2 \times 10^{19}$ cm^{-2} to $\sim 6 \times 10^{22}$ cm^{-2}. (*right*) Histogram of the widths of 90 filaments identified in the IC 5146, Aquila and Polaris regions (solid line filled in with solid orange). In addition, the distribution of Jeans lengths over the same regions shown (blue dashed line). The histogram of widths when alternative distances to these clouds are used is also shown (black dotted line). (Panels from Arzoumanian et al. 2011.)

Images like Fig. 3 are giving further insight into the formation of filaments. Fig. 4 (left) shows a curvelet component of the column density map of IC 5146, determined similarly to the one of Aquila shown in Fig.2. In this case, however, an automated cosmic web identification algorithm called DisPerSe (Sousbie 2011) has been used to identify 26 filaments threading the cloud, and the loci of the maximum column densities of each are shown as blue linear features across IC 5146 in Fig.4 (left). Interestingly, the filaments show a surprising similarity in width, i.e., ~ 0.1 pc. Following application of DisPerSe to the Aquila, Polaris and IC 5146 data, this common width was found in all cases. Fig.3 (right) shows a histogram of the widths found for 90 filaments identified in these three clouds, showing a strong peak at 0.1 pc. This near-constant value is surprising, as the column densities of the filaments themselves vary over 2.5 orders of magnitude and one might expect naively that widths would decrease as filaments grow in column density if they evolve through contracton. Indeed, the width distribution is much more sharply peaked than the wide and flat distribution of Jeans lengths for the cloud (also shown). We stress that widths were determined using the full, non-spatially decomposed column density maps, and the clouds differ in distance by a factor of ~ 4. (These widths are of course strongly dependent on assumed distances. The dotted histogram in Figure 3 (right) shows the width distribution given other potential distances; it still peaks at ~ 0.1 pc but much less sharply than before.)

As described in Arzoumanian et al., a common filament width may be the result of the turbulent formation of filaments, and their consequent evolution as mass accretes onto them. Namely, filaments may form in shocked regions resulting from

the collision of turbulent flows within clouds. In this scenario, the thickness of the shocked region, $\lambda \approx L/M(L)^2$, where L is the size of the impacting flow and M is the Mach number of the flow. From Larson's Laws, however, we expect $M(L) \propto L^{0.5}$, and so λ will be constant, and can be associated with the sonic scale where the 3D turbulent velocity approximately equals the sound speed, i.e., 0.05-0.15 pc as observed (see Heyer et al. 2009). After formation, the filaments may accrete surrounding material and maintain quasi-virial balance, as the kinetic energy of accreting material is transferred into the velocity dispersion of filament gas, σ_v. Hence, if Σ_o is defined as the column density of the filament, $\lambda = M_{line,vir}/\Sigma_o \approx \sigma_v^2/G\Sigma_o$ is constant since $\sigma_v \propto \Sigma_o^2$ as observed. Further work exploring the potential role of magnetic fields within this scenario is needed, however.

5. Conclusions

Herschel observations are revolutionizing our understanding of how small scale structures (filaments and cores) form in molecular clouds and how these structures may relate to the properties of stars that form out of them. This short contribution has summarized the earliest of conclusions drawn from the first far-infrared/submillimetre continuum data from the *Herschel* data of the Gould Belt Survey. In future, these conclusions will be tested against *Herschel* data from a dozen other nearby clouds, including the well-known clouds in Orion, Taurus, Perseus and Ophiuchus.

Acknowledgements

References

Alves J. F., Lombardi M., Lada C. J., 2007, A&A, 462, L17
Anathpindika S., 2011, NA, in press
André Ph., et al., 2010, A&A, 518, L102
Arzoumanian D., et al., 2011, A&A, 529, 6
Bergin E. A., Tafalla M., 2007, ARA&A, 45, 339
Bontemps S., et al., 2010, A&A, 518, L85
Chabrier G., 2005, in E. Corbelli et al., eds, The Initial Mass Function 50 years later, p. 41
Crapsi A., et al., 2007, A&A, 470, 221
Di Francesco J., et al., 2007, in B. Reipurth et al., eds, p. 17
Enoch M., et al., 2008, ApJ, 684, 1240

Evans N. J., II, et al., 2001, ApJ, 557, 193
Gould B. A., 1879, RNAO, 1, 1
Griffin M., et al., 2010, A&A, 518, L3
Heyer M., et al., 2009, ApJ, 699, 1092
Hildebrand R. H., 1983, QJRAS, 24, 267
Inutsuka S.-I., Miyama S. M., 1997, ApJ, 480, 681
Johnstone D., et al., 2000, ApJ, 545, 327
Johnstone D., et al., 2004, ApJ, 611, L45
Kirk H. M., et al., 2006, ApJ, 646, 1009
Könyves V., et al., 2010, A&A, 518, L106
Kramer C., et al., 1998, A&A, 329, 249
Kroupa P. 2001, MNRAS, 322, 231
Men'shchikov A., et al., 2010, A&A, 518, L103
Miville-Deschênes M.-A., et al., 2010, A&A, 518, L104
Motte F., André Ph., Neri R., 1998 A&A, 336, 150
Ostriker J., 1964, ApJ, 140, 1056
Pilbratt G., et al., 2010, A&A, 518, L1
Poglitsch A., et al., 2010, A&A, 518, L2
Reid M. A., et al., 2010, ApJ, 719, 561
Sadavoy S., et al., 2010, ApJ, 710, 1247
Salpeter E. E., 1955, ApJ, 121, 161
Sousbie T., 2011, MNRAS, 414, 350
Swift J. J., Williams J. P., 2008, ApJ, 679, 552
Ward-Thompson D., et al., 2007, in B. Reipurth et al., eds, Protostars & Planets V, p. 33
Ward-Thompson D., et al., 2010, A&A, 518, L92